Molecular Nature of the β Relaxation in Poly(methyl methacrylate) Investigated by Multidimensional NMR

K. Schmidt-Rohr,† A. S. Kulik, H. W. Beckham, A. Ohlemacher, U. Pawelzik, C. Boeffel, and H. W. Spiess*

Max-Planck-Institut für Polymerforschung, Postfach 3148, D-55021 Mainz, Germany

Received February 7, 1994; Revised Manuscript Received May 9, 1994®

ABSTRACT: The molecular motions underlying the dielectric and dynamic-mechanical β relaxation in poly(methyl methacrylate) (PMMA) have been elucidated in detail by means of two-dimensional (2D) and three-dimensional (3D) ^{13}C exchange NMR of the carboxyl moiety and 2D ^{2}H exchange NMR of the methoxy group. The identity of the motions observed by NMR and the β-relaxation dynamics is proved by the agreement of the measured correlation times. The selective-excitation "3D" NMR spectrum proves that, for every mobile side group, a relatively well-defined motion between two potential-energy minima occurs. The 2D spectral pattern shows that the OCO plane of the side group undergoes 180° (±20°) flips. Experiments with *m*ultiple *e*xchange and *s*elective *s*aturation for *a*nalysis of the *g*rowth of *e*xchange *s*ignals (MESSAGE) prove that the molecular motions responsible for the β relaxation are associated with a distribution of correlation times, which appears to be bimodal with both mobile and trapped side groups. Consistently, analysis of the integral 2D exchange intensity shows that around 330 K only about 50% of the side groups participate in the large-amplitude dynamical process on the time-scale of the β-relaxation correlation time. The 2D ^{2}H NMR spectra, while exhibiting narrowing due to methyl-group rotation around the O–CH_3 bond, exclude any significant motion of the methoxy group around the C–OCH_3 bond. Both the ^{13}C and the ^{2}H 2D NMR spectra provide compelling evidence that the side-group flip is accompanied by a main-chain rearrangement which can be characterized as a random rotation around the local chain axis with a 20° root-mean-square amplitude. This is ascribed to the fact that the asymmetric side group, after the flip, does not fit into its original environment. These findings explain both the dielectric and the dynamic-mechanical β relaxations of PMMA.

(1) Introduction

The β relaxation observed in poly(methyl methacrylate) (PMMA) by means of both dielectric and dynamic-mechanical measurements is often considered as the archetype of a localized (β) relaxation in polymers. With the maximum of the mechanical loss near 10 Hz at ambient temperature,[1] this β relaxation provides a mechanism for energy dissipation which can be linked to PMMA's favorable mechanical properties at and above room temperature (up to softening setting in near the glass transition temperature $T_g \approx 373$ K). Of a very similar nature as in PMMA are the β processes observed in other methacrylates, and possibly also those of acrylates and vinyl esters.

Since the β relaxation is very prominent in dielectric relaxation, it has traditionally been attributed to the carboxyl side group (see Figure 1) with its large dipole moment. Hindered rotation of the side group around the bond linking the main chain and the side group, possibly involving a 180° rotational jump, has been the favored explanation for the relaxation peak,[1] but its precise nature could not be determined, and large-amplitude rocking motions of the side group were never ruled out by experiment. In addition, it was usually not considered that the simple 180° flip entails steric problems: Because the side group is asymmetric (see Figure 1), after the flip it does not exactly fit in its original environment. This should be expected to complicate the motional process. Whether significant main-chain motions are involved in the β relaxation far below T_g, as has been suggested in the literature,[2–4] has not yet been determined by direct experimental evidence.[5,6] Other motions, such as a rotation of the methoxy group around the C–OCH_3 bond,[7] have also been postulated for PMMA below T_g.[8,9] It has also been argued that the β relaxation, rather than being due to a specific intramolecular motion, is generated by frozen-in density fluctuations which produce "islands of mobility".[10,11]

Two-dimensional (2D) exchange NMR[12–16] studies of polymers[16–18] have elucidated many details of the molecular reorientation geometry[14–19] of motions with correlation times in the range of 0.1 ms $< \tau <$ 10 s. While these methods have been exploited to study the α relaxations of amorphous and semicrystalline polymers in great detail, only a few exchange NMR studies on localized (β) relaxations have been reported.[20,21] However, in 1D NMR certain localized relaxation processes, in particular phenylene ring flips, have been observed in many materials via their effects on ^{2}H quadrupolar[22] as well as ^{13}C chemical shift[23] and dipolar line shapes.[24] Therefore, it is intriguing that to our knowledge the β relaxation in PMMA has not been detected in NMR spectra, in spite of its prominence in dielectric experiments.

In this paper, we apply 2D and selective-excitation 3D exchange NMR techniques to study the motion underlying the β relaxation in PMMA. We utilize ^{13}C chemical shift and ^{2}H quadrupolar anisotropies to probe complementary angular information. In this way, the question of possible coupling of main-chain and side-group motions can also be tackled. To this end, in addition to studying ^{13}C NMR of commercial materials, we have investigated samples isotopically enriched in ^{13}C at the carboxyl carbon site and in ^{2}H at the ester methoxy group. The 2D experiment elucidates the geometry of the reorientation and provides an estimate of the fraction of segments actually taking part in the dynamics.[16,19] The 3D exchange technique yields the number of potential-energy minima involved in the dynamics of the individual segments.[19,25,26] From the temperature dependence of the exchange-correlation time, the activation energy is determined in order to identify

* To whom correspondence should be addressed.
† Present address: Department of Chemistry, University of California, Berkeley, CA 94720.
® Abstract published in *Advance ACS Abstracts*, July 1, 1994.

0024-9297/94/2227-4733$04.50/0

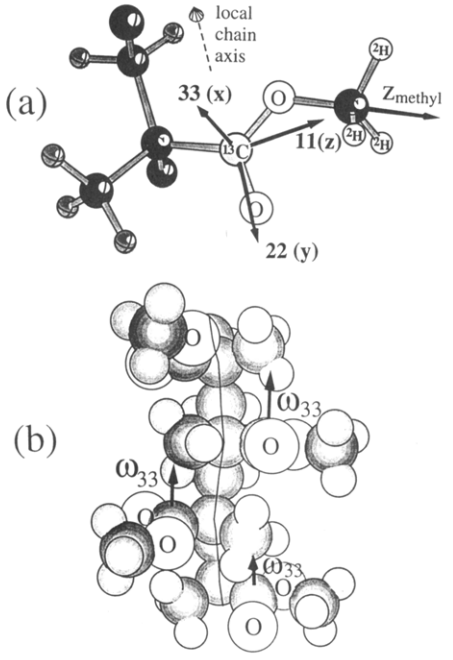

Figure 1. (a) Geometry of the PMMA repeat unit and the orientations of the NMR interaction tensors relevant in this study. The ω_{11}, ω_{22}, and ω_{33} axes of the carboxyl ^{13}C chemical-shift tensor are labeled "11", "22", and "33". In addition, these axes are designated by z, y, and x according to the alternative ω_z, ω_y, and ω_x nomenclature (see text). The ω_{33} axis is perpendicular to the OCO plane. This feature is common to all known carboxyl-group ^{13}C shift tensors. The C_3 axis of the rotating methyl group is the unique ("z_{methyl}") axis of the quadrupolar interaction of the deuterons, as indicated in the figure. (b) Typical chain segment in syndiotactic PMMA and syndiotactic sequencies of amorphous PMMA. The local chain axis is approximately perpendicular to the OCO planes, since the bulky but relatively flat side groups have a tendency to stack perpendicular to the local chain axis, to avoid the α-methyl groups of adjacent segments. Therefore, the ω_{33} axes, indicated by the arrows, are nearly parallel to the (local) chain axis. Note also that the OCH_3 groups project out of the "core" of the chain and will thus be surrounded by atoms of other chains. Consequently, the environment of each side group will be significantly asymmetric.

the reorientations observed by exchange NMR with the β-relaxation dynamics. Since several multidimensional NMR techniques are employed which are nonstandard or have not even been described before, a section is devoted to giving some NMR background before we discuss the specific results obtained on PMMA.

(2) Experimental Section

NMR. The ^{13}C spectra were acquired with cross polarization (contact time of 2 ms) and proton decoupling[27] in a variable-temperature ^1H–^{13}C probehead on a Bruker MSL-300 spectrometer operating at a ^{13}C resonance frequency of 75.47 MHz, with pulse lengths of 5 μs and recycle delays of 2 s. To obtain carboxyl powder patterns undistorted by the spectrometer deadtime, Hahn spin echoes were generated. The echo delay between the end of the cross-polarization period and the refocusing 180° pulse was $\tau = 50$ μs. The 2D spectra were measured off-resonance, so that only a single-phase dataset had to be acquired.[16,19] The irradiation frequency was set to ca. 85 ppm, between the signals of the carboxyl and aliphatic groups. Since the latter lack sufficient angular and spectral resolution, only the carboxyl regions of the spectra are shown below. Typically, 64 t_1 increments of 32 μs were sampled. Measuring times for a 2D spectrum ranged between 8 and 24 h.

The ^2H spectra were taken on a Bruker CXP 300 at 46 MHz in a variable-temperature ^2H probehead, with 90° pulse lengths of 3 μs. Data acquisition and processing were performed essentially as described in ref 14.

Table 1. Molecular Weights, Polydispersities, and Glass Transition Temperatures of the Investigated PMMA Samples.[a]

sample	M_n	M_w	M_w/M_n	T_g (°C)
unlabeled	1 490 000	2 150 000	1.44	116
$-^{13}COOCH_3$	55 500	112 000	2.02	128
$-COOC^2H_3$	48 800	94 500	1.94	122

[a] The molecular weight data were obtained from GPC using PMMA calibration. DSC diagrams were taken at a heating rate of 10 K/min.

Table 2. Stereoregularity of the Various Polymers As Obtained from High-Resolution ^1H NMR at 500.13 MHz Using Chlorobenzene-d_5 as Solvent at 100 °C

	diads[a]		triads[b]		
sample	m	r	mm	mr	rr
unlabeled	0.22	0.78	0.06	0.32	0.62
$-^{13}COOCH_3$	0.42	0.58	0.03	0.35	0.62
$-COOC^2H_3$	0.41	0.59	0.06	0.32	0.62

[a] Values obtained from the methylene signals. [b] Values obtained from the methyl resonances.

Samples. Natural-abundance PMMA samples were obtained from Röhm, Darmstadt. Molecular weight and tacticity information are given in Tables 1 and 2.

Synthesis of the Isotopically Labeled PMMA Samples. Methyl Methacrylate $^{13}COOCH_3$. The synthesis of the ^{13}C-labeled monomer was performed in a two-step reaction. In the first step, acetone cyanohydrin was reacted from acetone with ^{13}C-labeled sodium cyanide (purchased from Cambridge Isotopes) in the presence of 40% sulfuric acid at 10–20 °C.[28] The resulting acetone cyanohydrin has been isolated after extraction with diethyl ether by vacuum distillation (bp_{20} = 66–68 °C, n_D^{20} = 1.40). The yield was 68%.

The monomer was obtained from the acetone cyanohydrin after elimination of H_2O in the presence of fuming sulfuric acid at 60 °C, resulting in acetonitrile.[29] In order to avoid polymerization, hydroquinone was added as an inhibitor. The saponification of the nitrile and the esterification with methanol were performed without prior isolation of the nitrile. Methanol/water was added at a temperature of the oil bath of 110 °C (reaction temperature 90 °C). The mixture was then held at that temperature and stirred for 7–8 h. The methyl methacrylate monomer was isolated by steam distillation and successive extraction with diethyl ether and fractionated distillation (bp = 80.5 °C). The yield of the ester was 19%; a 20% residue of methacrylic acid was obtained.

Methyl Methacrylate $COOC^2H_3$. The deuterated monomer methyl methacrylate OC^2H_3 was obtained via the same reaction scheme. Methanol-d_3 was used in the esterification reaction.

Polymerization. The polymers were obtained by free-radical polymerization at 60 °C in toluene with 0.5 mol % azobis(isobutyronitrile) as initiator. They were then precipitated in cold methanol for purification. Yield: 70%. For making the ^{13}C-enriched PMMA sample, only 20% of the monomer was labeled; the remaining 80% monomer was commercial (Merck, Darmstadt) methyl methacrylate which was distilled prior to the polymerization. This 20% labeling was chosen in order to avoid homonuclear dipolar broadening of the ^{13}C spectra and to prevent exchange by spin diffusion from occurring within mixing times of less than 100 ms.

The molecular weights and the glass transition temperatures of the PMMA samples measured by GPC and DSC, respectively, are given in Table 1 and tacticities obtained from solution NMR spectra in Table 2. Prior to the NMR experiments all samples were melt pressed at 25 K above T_g for about 30 min.

(3) NMR Background

This section gives a short introduction to the aspects of solid-state NMR spectra that are relevant in this study. More detailed descriptions can be found in refs 14–19.

Angle-Dependent NMR Frequencies. Solid-state NMR methods can yield information on molecular reori-

entations due to the angle dependence of anisotropic NMR interactions. In order to elucidate rather subtle details of the complex dynamical processes responsible for the β relaxation of PMMA, a number of NMR experiments are employed. In fact, some of them have not been discussed before. Therefore, we give an outline of the NMR background needed to follow our arguments.

The NMR frequency reflects the orientation of a given molecular unit relative to the externally applied magnetic field $\mathbf{B}_0$ according to[30]

$$\omega_{aniso}(\theta,\phi) = \delta/2(3\cos^2(\theta) - 1 - \eta\sin^2(\theta)\cos(2\phi)) \quad (1)$$

Here, (θ,ϕ) are the polar angles of $\mathbf{B}_0$ in the principal-axes system of the ^{13}C chemical-shift or ^2H field-gradient tensor, whose orientation with respect to the molecular unit is an inherent property of every type of functional group and reflects its local symmetry (cf. Figure 1a). For deuterons in aliphatic C–^{2}H bonds, the field-gradient tensor is uniaxial and its unique principal axis is directed along the C–^{2}H bond. For the fast-rotating C^2H_3 group, the effective unique principal axis points along the C_3 rotation axis.[19,22] In carboxyl groups, for symmetry reasons one principal axis of the ^{13}C shift tensor must be perpendicular to the OCO plane; in general, it corresponds to ω_{33}, the most upfield tensor principal value,[31] which coincides with the right edge of the powder pattern; see Figure 3a. This has recently been confirmed by investigation of oriented PMMA.[32] The orientation of the two other axes within the OCO plane, to which they are confined by the ω_{33} direction, varies somewhat between different molecules, but in esters the ω_{22} axis is usually close to the C=O bond.[31] The simulated 2D exchange patterns shown below were obtained with an angle of 3° between the C=O bond and the ω_{22} axis.

For labeling of the principal values, we will use two conventions: The first convention labels the principal values downfield to upfield (from left to right) as ω_{11}, ω_{22}, and ω_{33}.[31] It is particularly useful for comparing the chemical-shift tensor orientations and principal values of similar segments (e.g., carboxyl groups). The other convention,[30] using the symbols ω_y, ω_x, and ω_z for the principal values, references them to the isotropic chemical shift as the null point of the frequency scale and then requires that

$$|\omega_y| \le |\omega_x| \le |\omega_z| \quad (2)$$

It is more suitable for the description and analysis of tensor orientations and reorientations. In particular, this convention makes sure that for uniaxial interaction tensors the unique axis is always the z principal axis.

The parameters δ and η in eq 1 are related to the principal values of the interaction tensor and the isotropic frequency ω_{iso} according to[19,30]

$$\delta = \omega_z$$

$$\eta = (\omega_y - \omega_x)/\delta \quad (3)$$

The deviation from uniaxiality, η, is negligible for spectra of ^{2}H in aliphatic C–^{2}H bonds ($\eta \sim 0$). In the fast-rotating methyl group, the averaged field-gradient tensor is also uniaxial, and its anisotropy parameter $\bar{\delta}$ is $-1/3$ of that of rigid C–^{2}H bonds.[22]

In an isotropic sample (a "powder"), segments with all possible values of θ and ϕ are present, giving rise to an inhomogeneously broadened powder spectrum with a characteristic line shape.[30] It extends from ω_{11} to ω_{33}, over a width of $\delta(3+\eta)/2$, with steep edges at ω_{11} and ω_{33} from which the intensity increases monotonically toward the maximum at ω_{22} (cf. Figure 3a). If reorientational motions set in with rates on the scale of the width ω_{11} to ω_{33} of the powder spectrum, the frequencies change during the acquisition of the NMR signal. This results in line-shape changes which contain some information on the rate and geometry of the motion.

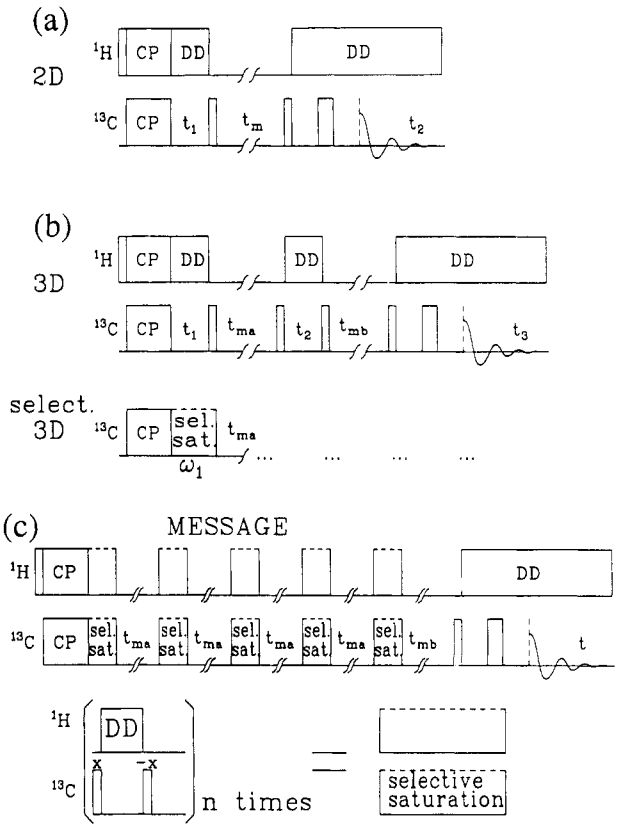

Figure 2. Pulse sequences of multidimensional exchange NMR as used for obtaining the ^{13}C spectra shown in this paper. ^{13}C magnetization is created by cross polarization (CP) from protons, which are then decoupled by high-power irradiation (dipolar decoupling, DD). Before detection, a Hahn spin echo is generated by means of a 180° pulse, in order to overcome spectrometer deadtime problems. (a) Pulse sequence for two-dimensional (2D) exchange NMR, with incremented evolution time t_1, mixing time t_m, and detection time t_2. (b) Three-dimensional (3D) exchange NMR with two mixing times, t_{ma} and t_{mb}. The angle-dependent frequency is measured three times by incrementing t_1 and t_2 and detecting during t_3 in a full 3D experiment. In a "selective 3D" experiment, the frequency ω_1 is labeled by selective saturation of the rest of the spectral intensity. (c) Multiple exchange with selective saturation for the analysis of the growth of exchange (MESSAGE). For the selective saturation (abbreviated "sel. sat." in the figure), the SELDOM pulse sequence[33] as indicated at the bottom of the figure was employed. For the first selection-saturation pulse pair, the 90° pulse is replaced by the cross-polarization sequence.

2D Exchange NMR. The principle of two-dimensional exchange NMR[12] consists of the detection of slow reorientations that occur during a mixing time t_m by measuring the angular-dependent NMR frequencies before and after t_m.[14,16] The corresponding pulse sequence is shown in Figure 2a. The 2D frequency spectrum $S(\omega_1,\omega_2;t_m)$ is generated by two successive Fourier transformations over t_1 and t_2.[12,13] It represents the probability of finding a unit with a frequency ω_1 before t_m and with frequency ω_2 afterward.[15] If no reorientation, and consequently no frequency change, takes place during t_m, the spectral intensity is confined to $\omega_1 = \omega_2$, the diagonal of the

frequency plane. *Large-angle* reorientations usually give rise to intensity in large parts of the frequency plane.[14] Conversely, for anisotropic reorientations by *small angles*, the signal appears close to the diagonal, with a position-dependent broadening of the diagonal spectrum. Its most prominent effect is a change in the line shape along the diagonal. The broadening is usually least pronounced at the edges of the powder spectrum, where the angular dependence of the frequency vanishes to first order,[19] so that these edges remain higher than the other, more strongly broadened regions along the diagonal.

For the understanding of the PMMA ^{13}C spectra shown below, it is important to recognize how various motional processes can be distinguished due to their specific effects on the 2D intensity distribution.[19] The analysis is particularly straightforward if the symmetries of the nuclear interaction tensor and the segmental reorientation are related. For instance, if the effective direction of a principal axis remains invariant in the motional process, no exchange occurs at the corresponding frequency $\omega_{\alpha\alpha}$, such that the spectral intensity remains on the diagonal where it produces a notable extra peak compared to the rest of the spectrum with the intensity spread out into the 2D plane. Such invariance can result from a rotation around the corresponding principal axis. Due to the second-rank tensorial nature of the interaction, $\omega_{\alpha\alpha}$ remains also unchanged under an inversion of the α principal axis by a 180° flip of the segment.

3D Exchange NMR. The 2D exchange technique can be extended to 3D exchange NMR, where the orientation-dependent frequency is observed three times.[25,26] The 3D pulse sequence Figure 2b contains two mixing times t_{ma} and t_{mb}, two incremented evolution times t_1 and t_2, and the detection period t_3. The 3D NMR spectrum resulting from Fourier transformation over t_1, t_2, and t_3 provides useful information on the sequence of jumps. In particular, it makes it possible to detect distinct signals from jumps back to the start position. The full potential of 3D exchange NMR and several experimental examples are discussed in ref 19.

3D exchange spectra are most conveniently analyzed in terms of 2D cross sections at a constant ω_1. These 2D slices can also be measured individually by replacing the first evolution time t_1 by selective excitation of a frequency ω_1.[25] For technical reasons discussed below, this approach has been taken in this paper. For the selection of a relatively narrow band of frequencies we have employed the SELDOM (chemical-shift filter) technique.[33] Thus, an ensemble of molecules with frequency ω_1 is labeled by this selection, which is followed by a mixing time t_{ma}, during which exchange to other frequencies can occur. This exchange intensity is monitored in the evolution period of an ensuing 2D experiment. If during its mixing time t_{mb} a second frequency change occurs, it will be detected as an off-diagonal intensity in the (ω_2, ω_3) 2D spectrum that is acquired. In particular, if the segments return to the orientations they had taken before t_{ma}, their detection frequency ω_3 will be equal to the initial frequency ω_1, so they produce contributions on the straight line $\omega_3 = \omega_1$ in the (ω_2, ω_3) plane (a return-jump ridge). Signals that do not exchange during t_{mb} appear on the diagonal $\omega_3 = \omega_2$ of the (ω_2, ω_3) plane. For an exchange process between n sites, n ridges would be expected in the region $\omega_2 \neq \omega_1$ of the (ω_2, ω_3) plane. For small angular step diffusive reorientations, which can be considered as an exchange process between an unlimited number of closely-spaced sites, a broadened diagonal ridge and no return-jump ridge at $\omega_3 = \omega_1$ would be observed. It is the signature of the two-site exchange that only the diagonal ridge and the return-jump ridge are observed since only two orientations and corresponding frequencies are taken on by each segment. In the limit of long mixing times such that $\tau \ll t_{mb}$, these two ridges will have equal integral intensities, and their spectral line shape will be the same, if the two exchanging sites are equivalent.

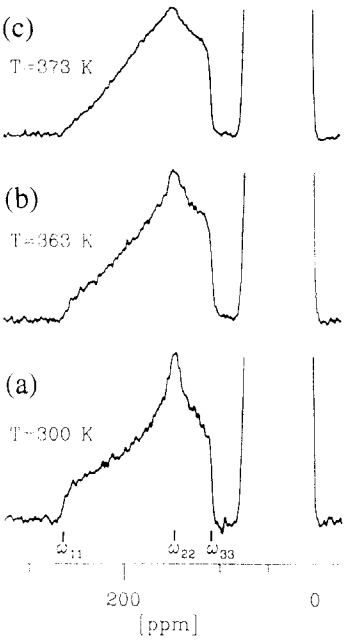

Figure 3. Temperature dependence of carboxyl ^{13}C (natural-abundance) NMR powder spectra in PMMA, taken with Hahn echo delays of $2\tau = 100$ μs. At 300 K, a typical chemical-shift powder pattern is observed. The line-shape changes observed at higher temperatures prove large-angle motions, but details cannot be reliably extracted due to the relatively small number of significant features in these one-dimensional spectra.

Several full 3D exchange NMR spectra reflecting the α processes in various polymers have been successfully measured and have been useful for studying orientational memory and sequences of jumps.[19,26] However, for the β process in PMMA a selective 3D experiment is preferable for several reasons. We are particularly interested in finding out whether or not the side-group motion has two-site jump characteristics. To prove or disprove a two-site jump process, a single, suitably chosen 2D slice is fully sufficient and more convenient in terms of data processing. In addition, the height of the exchange signal in PMMA is only ~2% of the height of the maximum on the diagonal and thus susceptible already to phasing artifacts on a 2% level which are difficult to avoid in full 3D spectra. Technically, in the selective-excitation 3D experiment applied to PMMA it has proven sufficient and advantageous in terms of phase-error suppression, to measure a single cosine dataset although the selected band is on resonance.[16,19] The resulting lack of $\pm\omega_2$ frequency discrimination does not introduce any ambiguities for the $\omega_3 = \omega_2$ and $\omega_3 = \omega_1$ ridges in the relevant region defined by $\omega_2 \neq \omega_1$ in the (ω_2, ω_3) frequency plane.

MESSAGE Experiment. In glassy systems, due to the variations in the local environments, the correlation times for molecular dynamics often exhibit broad distributions. So far, in the slow-motion regime, which is particularly relevant for motions of polymers, only the reduced-4D experiment[34,35] could provide information on the nature of such distributions of correlation times. In this paper, we introduce a new simple approach to tackle this problem by *m*ultiple *e*xchange and *s*elective *s*aturation for *a*nalysis of the *g*rowth of *e*xchange *s*ignals (MESSAGE).

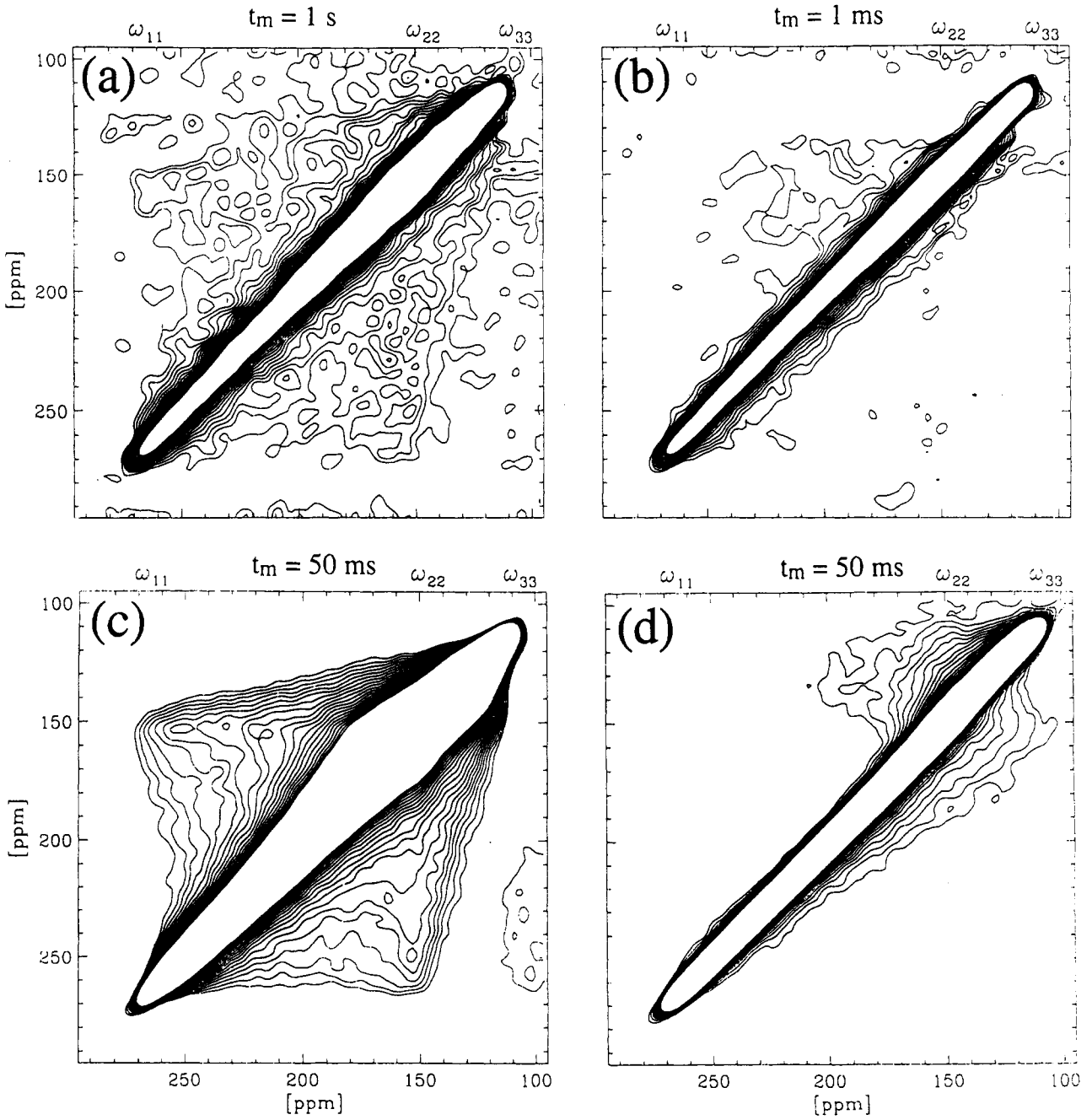

Figure 4. ^{13}C carboxyl 2D exchange NMR spectra of PMMA. (a) Spectrum of commercial PMMA (^{13}C in natural abundance) taken with a mixing time of t_m = 1 s at T = 323 K. The measuring time was 16 h. Twenty contour lines are plotted between 1% and 15% of the maximum intensity. The high intensity along the diagonal is shown white since it is higher than the highest contour level. (b) Corresponding diagonal spectrum with t_m = 1 ms for comparison. In the spectrum of b compared to that of a, indications of exchange intensity are found in a large area of the frequency plane, but both the signal-to-noise ratio and spectral resolution are insufficient for a detailed analysis of the underlying motional process. (c) 2D spèctrum of PMMA with 20% of the side groups ^{13}C labeled at the carboxyl carbon. T = 333 K and t_m = 50 ms. The contour lines are linear between 0.5% and 5% of the maximum intensity. (d) Diagonal spectrum of the same ^{13}C-labeled material, taken with the same t_m = 50 ms but at a lower temperature of T = 233 K. Only a minimal exchange intensity is observed, which proves the ^{13}C spin diffusion is negligible for the mixing time of 50 ms.

Its principle is related to saturation-transfer experiments,[36] but the great potential for proving and analyzing heterogeneous distributions of correlation times has not yet been recognized. The pulse sequences (Figure 2c) consist of n cycles of selective saturation sequences, each of which leaves only a narrow band of frequencies, usually at ω = 0 (on resonance), unsaturated, and each of which is followed by a mixing time t_{ma}. The sequence is concluded by a mixing time t_{mb}, which is usually longer than t_{ma}, and followed by a read-out 90° pulse and (1D) signal detection.

If the mixing times t_{ma} are chosen much shorter than the shortest relevant correlation time, no exchange occurs during t_{ma} and a selective 1D exchange NMR spectrum with mixing time t_{mb} results, which is equivalent to a cross section, at the ω_1 value corresponding to the selected band, through a 2D exchange spectrum with the same mixing time t_{mb}. Next, we assume that segments with long and short correlation times are present in the sample (a heterogeneous correlation-time distribution). When the mixing times t_{ma} are chosen to be comparable to the short correlation times, many of the corresponding signals change their frequencies during t_{ma} and are suppressed in the next selective-saturation step. After many cycles, these signals are suppressed very efficiently, while those of the slowly reorienting segments are retained and selectively observed in the 1D spectrum taken at the end of the

sequence. The decrease of the exchange intensity for a given $t_{mb} > t_{ma}$ as a function of nt_{ma} then provides direct information on the characteristics of the heterogeneous distribution of correlation times. Finally, in a homogeneous system, the shape of the MESSAGE spectrum does not depend on t_{ma}, and the overall intensity is reduced exponentially with nt_{ma}.

In order to appreciate the information content of the MESSAGE experiment, it should be noted that the 1D exchange spectrum after n selective-saturation and exchange cycles is the 1D slice $S(\omega_n) = S_{n+1}(\omega_1,\omega_1,\omega_1,\omega_1,\omega_1,\omega_1,...,\omega_1,\omega_1,\omega_{n+1})$ of the $(n+1)$-dimensional exchange spectrum $S_{n+1}(\omega_1,\omega_2,\omega_3,\omega_4,\omega_5,...,\omega_n,\omega_{n+1})$.

In the MESSAGE spectra shown below, the SELDOM pulse sequence[33] is used for selective excitation. It consists of several cycles of two pulses and two delays. Each cycle consists of a 90° excitation pulse, a certain precession period t_{spr} during which the isochromats are separated, and a flip-back 90° pulse that brings the on-resonance component fully back to the axis, but only a fraction $\cos(\omega t_{spr})$ of other isochromats. The transverse magnetization components $\sin(\omega t_{spr})$ are then destroyed by T_2 relaxation during a delay without ^{1}H decoupling, which is the mixing time t_{ma} in the MESSAGE experiment. Though each individual cycle does not provide complete selective saturation, the effect of short and long t_{ma} times is essentially the same as described above where perfect selective saturation was assumed in each step. The duration of the proton-decoupled precession delays in the SELDOM pulse sequence can be increased within each pulse train to enhance the selectivity: The longer delays result in sharper selection, while the shorter delays suppress the undesired signals over a wider range.

(4) Results and Discussion

Temperature Dependence of Motional Rates from 1D and 2D ^{13}C NMR. In Figure 3, 1D natural-abundance ^{13}C powder NMR line shapes of the carboxyl-group chemical-shift tensor are shown as a function of temperature. At room temperature, a nearly regular powder spectrum is found, with ω_{11} = 268 ppm, ω_{22} = 150 ppm, and ω_{33} = 112 ppm (±3 ppm), equivalent to ω_{iso} = 177 ppm, ω_z = 91 ppm, ω_y = −27 ppm, and ω_x = −65 ppm. As the temperature is raised, increasingly pronounced line-shape changes are observed. As mentioned above, this is indicative of large-amplitude motions with rates exceeding the width of the powder spectrum (10 kHz). These are fully consistent with the rates of nearly 10000/s determined around 373 K for the β relaxation by dielectric and dynamic-mechanical measurements.[1,37] At this point, it does not appear advisable to attempt to extract geometric information out of these one-dimensional spectra. In particular, the line shape cannot be described by a single η and $\bar{\delta}$, as would be the case for a simple process in the fast-exchange regime defined by a rate $1/\tau \gg \delta$ common to all side groups. This shows that the motional rate $1/\tau$ has not yet reached this fast regime, that the motion is not homogeneous for all molecules, or both. Since distributions of correlation times and of reorientation angles are indeed to be expected in a disordered glass such as PMMA, the number of parameters entering the simulation of the 1D spectra would be too large to produce a significant result. Nevertheless, after characterization of the reorientation geometry by 2D and 3D NMR, the 1D line shape can provide additional information about the dynamics. This will be discussed below.

Below the temperature where appreciable line-shape changes set in, the dynamics is in the slow-motion limit

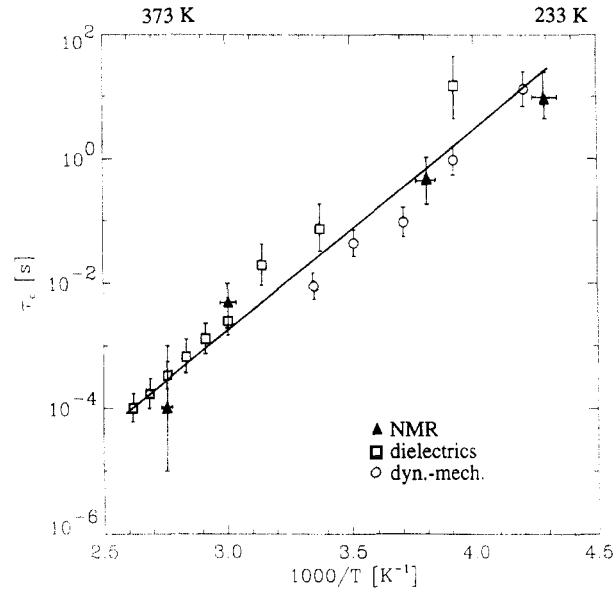

Figure 5. Arrhenius plot of correlation times of the β-relaxation dynamics in PMMA, as estimated from 1D and 2D NMR spectra, compared to both dielectric data obtained from the β-relaxation loss maxima[1,37] and relaxation times from dynamic-mechanical studies.[11]

$1/\tau \ll \delta$ which can be studied well by 2D exchange NMR. Parts a and b of Figure 4 compare 2D ^{13}C spectra taken at T = 323 K, one with a long mixing time of 1 s and the other with t_m = 1 ms only. While no off-diagonal intensity above a level of 1% of the maximum is detected for the short mixing time, for t_m = 1 s indications of exchange intensity far off the diagonal are found slightly above the noise level.

It is obvious that an analysis of the details of the molecular reorientation from the 2D NMR spectrum requires an order-of-magnitude enhancement of the signal-to-noise ratio compared to the spectrum of Figure 4a. This was achieved by ^{13}C-labeling of 20% of the carboxyl carbons. The 2D NMR spectrum from such a sample at T = 333 K and t_m = 50 ms is shown in Figure 4c. The exchange pattern is seen clearly now, exhibiting intensity far off the diagonal. This indicates large frequency changes, which correspond to large reorientation angles. A large portion of the frequency plane exhibits intensity, but not all of it, which proves that the motion is not isotropic. The overall shape of the spectral intensity is the same as in the spectrum from ^{13}C in natural abundance shown in Figure 4a; the 1D spectra of the labeled and unlabeled samples also exhibit the same temperature dependence. This as well as the purely diagonal spectrum obtained at the lower temperature of 233 K and t_m = 50 ms (Figure 4d) shows that the exchange intensity in Figure 4c is not generated by ^{13}C spin diffusion but is indeed due to the same motional process as in commercial PMMA.

The motional rates of the large-angle reorientation process were determined from the mixing-time dependence of the exchange intensity found at different temperatures.[12,13,19] At higher temperatures they can be estimated from the onset of 1D line-shape changes, where the rate $1/\tau$ is comparable to the anisotropy δ. Figure 5 displays these data in an Arrhenius plot together with average correlation times obtained from dielectric[1,37] and dynamic-mechanical[11] relaxation. The straight line in the plot corresponds to an activation energy of 65 kJ/mol. The good agreement of the correlation times around and above 300 K shows that the motion detected by NMR is indeed directly related to the β relaxation. The nature of the distribution of correlation times is treated below.

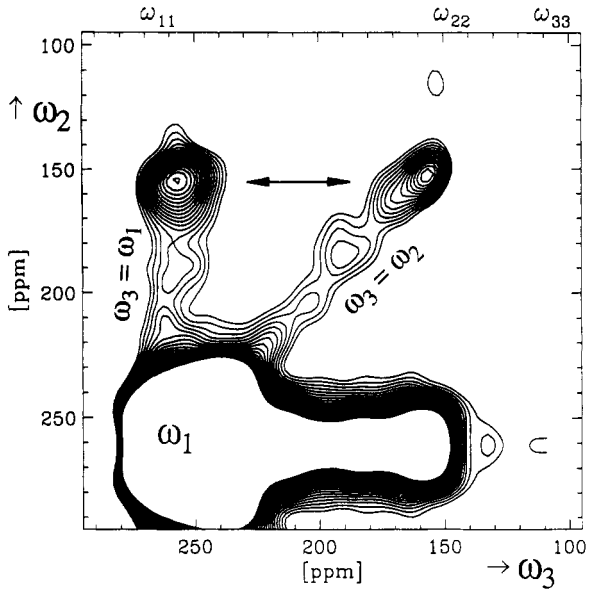

Figure 6. Selective-excitation 3D exchange ^{13}C NMR spectrum of the labeled carboxyl groups at T = 333 K and mixing times t_{ma} and t_{mb} = 50 ms. The selected ω_1 frequency is located at 260 ppm, near the low edge of the carboxyl powder pattern. The contour lines cover the range from 0.25% to 1.5% of the spectral maximum. Only two straight ridges, along $\omega_3 = \omega_2$ and $\omega_3 = \omega_1$, are observed in the relevant region of $\omega_2 \neq \omega_1$. Their similar spectral shapes and intensities prove that, in spite of the diffusive appearance of the 2D exchange spectrum in Figure 4c, the reorientation of each segment involves only two relatively well-defined potential-energy minima.

Geometry of Large-Angle Ester-Group Motions. As noted above, the simplest picture of the ester-group motion considers a rotation by 180° around the C–COO bond, which corresponds to a two-site jump. However, the diffuse intensity distribution in the experimental spectrum of Figure 4c might rather suggest a more or less isotropic diffusive motion of 25% of the side groups, while the rest would be quite rigid and give rise to the relatively sharp diagonal portion of the 2D spectrum. On the other hand, the ω_{33} frequency is invariant in the motional process. This is deduced from the 2D spectrum of Figure 4c, where the cross section through the spectrum of $\omega_1 = \omega_{33}$ has only intensity for $\omega_2 = \omega_{33}$. With the ω_{33} axis perpendicular to the backbone-side-group C–C bond,[32] the invariance of ω_{33} requires an anisotropic rotation around this axis, and/or a two-site 180° rotational jump around the C–COO bond, which only inverts the ω_{33} axis without changing the NMR frequency of eq 1.

That the dynamics indeed involves such two-site jumps can be corroborated by 3D exchange NMR. Figure 6 displays a spectrum equivalent to a two-dimensional slice at fixed ω_1 through a 3D spectrum, obtained in a selective-excitation 3D experiment as described above. The spectrum was recorded at T = 333 K and mixing times $t_{ma} = t_{mb}$ = 50 ms, corresponding to the 2D spectrum in Figure 4c. The selected ω_1 frequency was set to 260 ppm, near ω_{11}, the low edge of the carboxyl powder pattern, since the overlap of diagonal and exchange intensity is minimal in the corresponding slice of the 2D spectrum. Two well-resolved straight ridges are observed in the (ω_2, ω_3) plane, along the diagonal $\omega_3 = \omega_2$ and along the $\omega_3 = \omega_1$ line. As discussed above in section NMR Background (3D Exchange NMR), this proves that the reorientation of each segment involves only two sites, i.e., two relatively well-defined potential-energy minima in spite of the diffusive appearance of the 2D exchange intensity in Figure 4c. Thus, the featureless exchange intensity in the 2D NMR spectrum results from a broad distribution in the relative orientations of these pairs of potential-energy minima. This arises from the fact that different side groups have different environments in the glassy state, requiring varying degrees of rearrangement of the main chain in the energy minimization after the jump (see below).

In order to analyze the geometries of the two-site jumps in more detail, we compare the experimental 2D NMR spectrum of Figure 7a to simulated spectra for various motional models (Figure 7b–d). The simulated 2D exchange NMR spectrum resulting from 180° side-group flips without main-chain motion is plotted in Figure 7b. The simulation shows a pronounced elliptical, nearly circular ridge, which is, however, absent in the experimental 2D spectrum. There, except for straight ridges tapering at the ω_{33} end of the spectrum, the exchange intensity is rather featureless. The circular ridge does not broaden appreciably even when assuming a distribution of the rotation angle around 180°. In fact, such a distribution with a root-mean-square (rms) amplitude of σ = 25° (corresponding to a full width at half-maximum of nearly 60°) was assumed in simulating the spectrum shown in Figure 7b. An upper limit of σ = 40° for these deviations is established by detailed line-shape analysis, in particular by considering the approximate invariance of the ω_{33} frequency in the 2D spectrum. Distributions in the rotational angle therefore cannot be invoked as the major source of the smearing-out of the exchange pattern.

In summary, we have shown here that the side-group motion occurs through large-angle flips between two sites, which are approximate 180° flips around the C–C bond connecting the main chain and side group, but that additional degrees of freedom must also be involved.

Coupling of the Side-Group Flips to Rotations around the Local Chain Axis. Because the ω_{33} and ω_{22} values are quite similar for the carboxyl chemical-shift anisotropy in PMMA, and since the ω_{33} axis is not involved in the exchange process, the exchange intensity mainly reflects the reorientation-angle distribution of the ω_{11} (ω_z) axis of the ^{13}C chemical-shift tensor. The featureless experimentally observed 2D intensity distribution in Figure 7a indicates a wide reorientation-angle distribution for the ω_z axes. As discussed above, simulated 2D spectra such as that of Figure 7b show that deviations of the flip angle from a central value of 180° do not cause such a broadening in the spectral region between ω_z and ω_y.

However, a distribution of rotation angles around the ω_{33} axis, which is perpendicular to the OCO plane, is very effective in broadening the exchange features in the region between ω_{11} and ω_{22}, while producing no exchange at ω_{33}. Structural studies,[32,38,39] and simulations[40] have shown that the normal of the OCO plane is parallel to the local chain axis within about 20°, as indicated in Figure 1. The amplitude of these restricted rotations around the local chain axis that accompany the 180° side-group flips is σ = 20° ± 7°, as estimated from the direct analysis of the ω_z-edge slice $S(\omega_1{=}\omega_z,\omega_2)$ of the 2D exchange NMR spectrum[16,41] and confirmed quantitatively by comparison of experimental and simulated 2D spectra (Figure 7a,c, respectively). We thus conclude that the 180° flip of the carboxyl side group must be coupled to significant rotations around the local chain axis.

As schematically indicated in Figure 8a–c, due to the asymmetry of the side group it is indeed expected that a rotation of limited amplitude around the normal of the OCO plane accompanies a side-group 180° flip. As shown in Figure 8b, a simple 180° flip without main-chain readjustment will in general lead to steric clashes of the

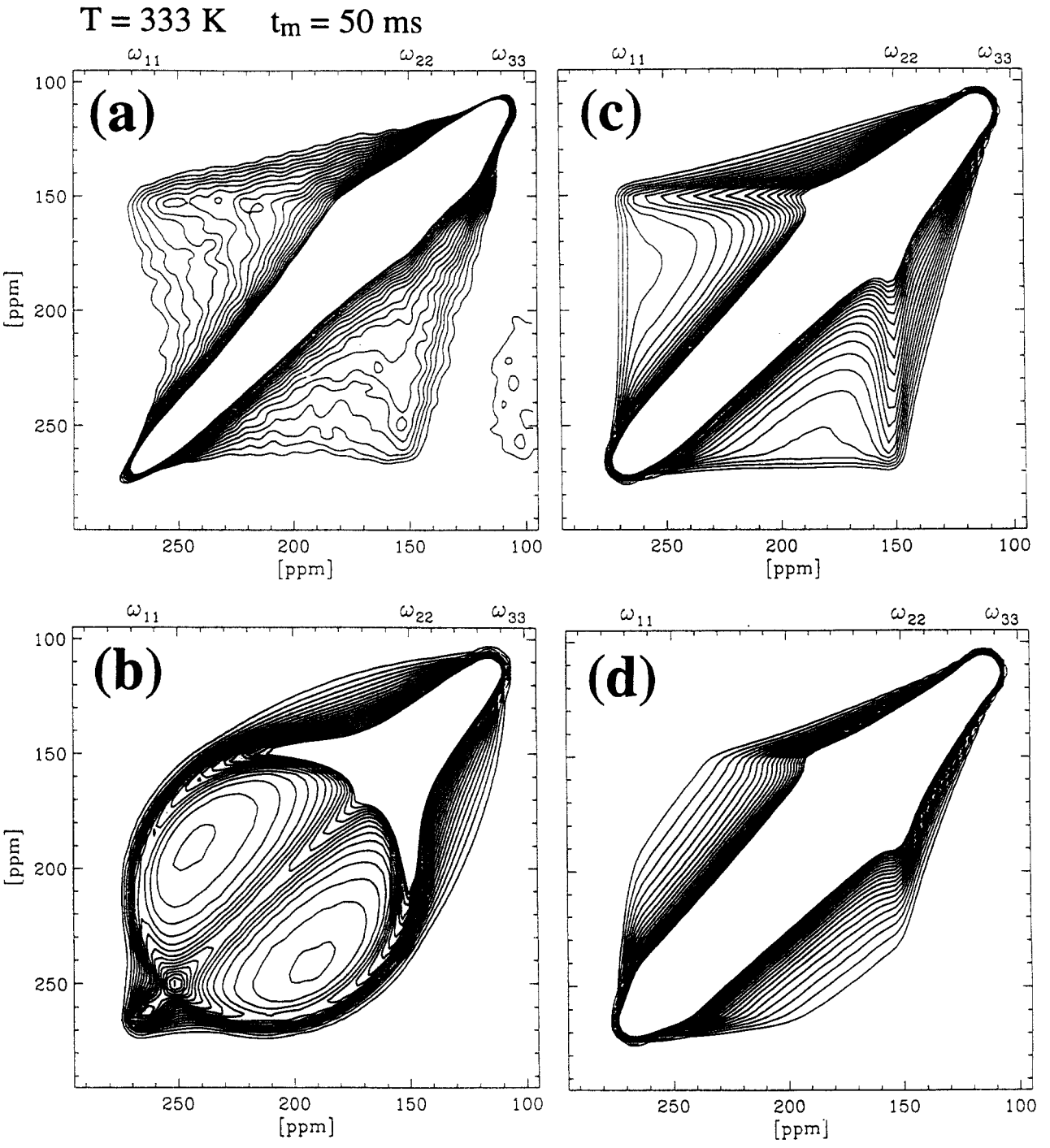

Figure 7. (a) 2D exchange ^{13}C NMR spectrum of PMMA with 20% of ^{13}COO-labeled side groups. T = 333 K and t_m = 50 ms. (b) Attempted simulation of the 2D spectrum in a assuming a Gaussian distribution of side-group flip angles of ±25° root-mean-square amplitude (i.e., 60° full width at half-maximum) centered on 180°. The pronounced elliptical ridge is not observed experimentally. (c) Best simulation of the spectrum in a, with a 180° ± 10° flip angle and a concomitant rotation around the ω_{33} direction (local chain axis) with a root-mean-square amplitude of ±20°. (d) Unsatisfactory simulation which results for a rocking motion without 180° flips, i.e., when only rotations around the ω_{33} direction (local chain axis) with a root-mean-square amplitude of ±25° are assumed.

OCH_3 group with surrounding units. Figure 8c indicates how these can be avoided by a ~20° rotation around the normal of the OCO plane, which is approximately parallel to the local chain axis. Then, only slight changes in the environment are necessary to accommodate the asymmetric side group after the 180° flip.

In order to corroborate this picture, we have analyzed the β-relaxation dynamics further via the anisotropic quadrupolar interaction of ^2H nuclei in selectively deuterated OCH_3 groups in PMMA. First of all, the quadrupole-coupling constant of $4\delta/3$ = 53 kHz, obtained from the splitting δ of the two horns of the Pake powder spectrum as in Figure 9, must be attributed solely to the fast three-site jumps of the methyl group ("methyl-group rotation") and excludes any other fast large-amplitude motion. The C_3 axis of the methyl group is the unique principal axis of the motionally averaged quadrupolar interaction whose further slow reorientation can be observed by 2D exchange NMR spectroscopy. In the ^2H 2D exchange spectrum of Figure 9, the exchange intensity is confined to the region around the spectral diagonal, despite the fact that this spectrum was recorded at T = 355 K and a mixing time t_m = 500 ms, much longer than the correlation time of the side-group motion (cf. Figure 5). First of all, this shows that indeed no large-angle rotations around the C–OCH_3 bond are activated. It also

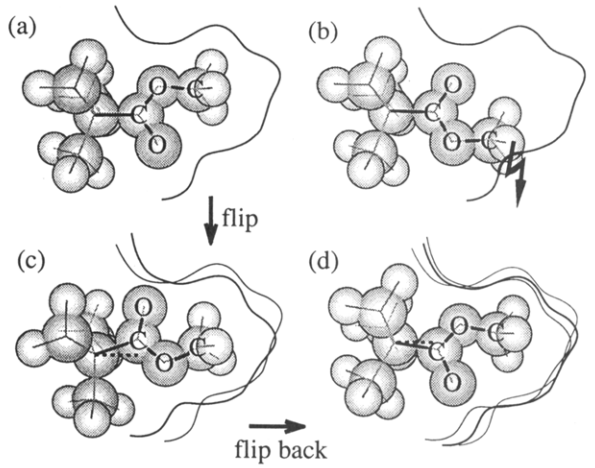

Figure 8. Schematic sketches of the dynamics of the asymmetric side group in its correspondingly asymmetric environment (cf. also Figure 1b). (a) Initial side-group orientation. (b) Steric clash with the environment if an exact 180° flip without main-chain motion is assumed. (c) To fit the asymmetric side group into the volume that it had occupied before the flip, a twist around the local chain axis is required. This in turn slightly deforms the environment. (d) A second jump takes the group back close to its original orientation in a, but not exactly, due to the previous change in the environment in c, which is enhanced by rotation of other side groups that make up that environment. Rearrangements of the main chain by neighboring flipping side groups will also induce such an effect of an effective small-angle rotation around the local chain axis.

implies that the side-group flips detected in the ^{13}C 2D spectra must leave the quadrupolar frequency nearly invariant. Within the constraints given by the chemical structure, this means that the direction of the C_3 axis of the OCH_3 moiety, which is the z principal axis of the quadrupolar interaction of the rotating methyl group, must be nearly parallel to the axis of the 180° flip motion. The O–CH_3 bond probe by ^2H NMR can only be nearly parallel to the C–C bond linking the carboxyl group to the polymer backbone if the side-group conformation is close to trans (cf. Figure 1a), which is in agreement with the accepted interpretation of the X-ray data of oriented PMMA.[38,39] Thus, the ^2H 2D spectra are insensitive to the 180° flip motion itself, probing quite selectively the additional rotational dynamics around the chain axis. The exchange intensity observed relatively close to the diagonal can thus be attributed to the rotations around the chain axis by about 20° as also deduced from the ^{13}C 2D NMR spectra. A detailed discussion of the reorientational angle distribution is given below (cf. Figure 13).

Our analysis shows that different side groups in the glassy polymer undergo motions with different overall reorientation angles, due to differences in the local environments. This is also apparent in the line shapes of the 1D ^{13}C NMR spectra at higher temperatures (see Figure 3). For rates in the fast-exchange limit of $1/\tau \gg \delta$, the superposition of powder patterns for the different motional geometries, instead of producing a single motionally narrowed powder pattern, results in a distinctive line shape of a hypothetical 1D ^{13}C NMR spectrum as shown in Figure 10. Indications of the linear slope at the low-field wing of the spectrum (near ω_{11}) and increased relative intensity near the ω_{33} end of the spectral range are actually visible in the experimental 1D spectra of Figure 3. The pure β relaxation cannot be investigated at significantly higher rates and temperatures because the characteristics of the motion change above the glass transition temperature and finally the α and β processes merge.[1] These aspects of the motional behavior are treated in companion papers on poly(ethyl methacrylate) (PEMA) dealing with highly anisotropic chain motion[42] and the coupling between the α and the β process.[43]

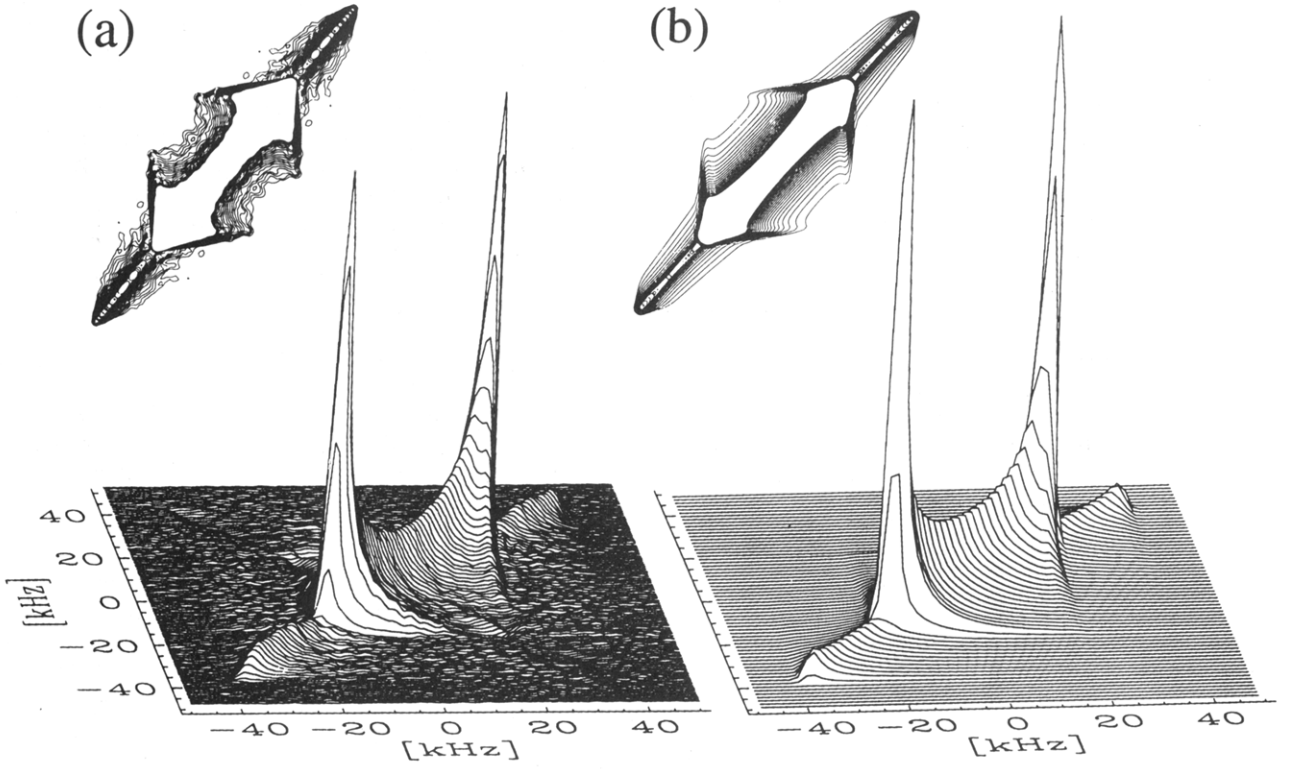

Figure 9. 2D ^2H NMR spectrum of PMMA deuterated in the OCH_3 group. (a) Experimental spectrum at T = 355 K and t_m = 500 ms. The absence of further narrowing of the powder pattern and the lack of exchange far off the diagonal excludes both fast and slow rotation of the methoxy group around the C–OCH_3 bond. (b) Corresponding simulation, with exchange generated by motions around the local chain axis. The full reorientation angle distribution is shown and analyzed in Figure 13.

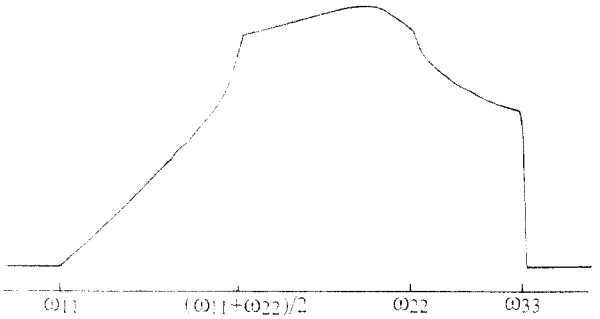

Figure 10. Hypothetical fast-exchange 1D ^{13}C NMR spectrum for the motional model underlying the 2D exchange simulations shown above. The motional rates have been extrapolated into the fast-exchange limit, where the rates $1/\tau$ are much larger than the anisotropy δ. Certain similarities with the spectrum in Figure 1c are apparent, even though the motional rates there do not fully reach the fast-exchange regime.

Heterogeneity of Rates. Integration of the experimental exchange intensity of the ^{13}C 2D NMR spectrum at T = 333 K, where $t_m/\tau \approx 5$, shows that the integrated exchange intensity makes up 25 ± 10% of the total. The relatively large uncertainty is mainly due to the overlap with the diagonal ridge in the spectrum. In a symmetric two-site jump process as indicated by the 3D experiment, at least half of the intensity is found on the diagonal for any mixing time. This means that 2(25 ± 10)% of the side groups participate in the exchange process on the time scale of the correlation time of the β process. The remaining 50 ± 20% which are slow on that time scale must be trapped in environments with higher activation barriers. The same fractions of trapped and mobile side groups also provide a good fit of the ^2H 2D spectrum (see Figures 9 and 13).

Such a heterogeneous distribution of correlation times can be proved without any assumptions by the MESSAGE experiment in ^{13}C NMR. As shown in Figure 11, multiple exchange and selective saturation suppress the relative fraction of the exchange intensity by a factor of 2, while the overall intensity is reduced only by a factor of 1.4 (the total reduction factor for the exchange intensity is 2 × 1.4 = 2.8). As discussed above, this is direct proof of a heterogeneous distribution of correlation times.

For a two-site exchange process, the exchange intensity can reach a maximum of 50% only if the two sites are energetically equivalent. Indeed, the observed exchange intensity in the range 140–230 ppm is only 25%. This could be due to unequal depths of the two potential-energy minima. If this were the case, the exchange intensity in the MESSAGE experiment would not be reduced by multiple saturation of the exchange intensity. Thus, the relative exchange intensities in parts a and b of Figure 11 would be the same. Since the experimentally observed suppression of the exchange intensity by the MESSAGE experiment is not complete (Figure 11b), energetic inequivalence of the two side-group orientations as required by the asymmetry of the PMMA side group may be partially responsible for the low exchange intensity. On the other hand, the suppression of the exchange intensity by a factor of 2 in the MESSAGE spectrum indicates that the energy-difference effect does not dominate over the effect of the heterogeneous distribution of correlation times. Similarly, in the selective 3D spectrum of Figure 6 the nearly equal intensities of the two ridges corresponding to the two sites are evidence for a relatively small energetical difference between the two side-group orientations.

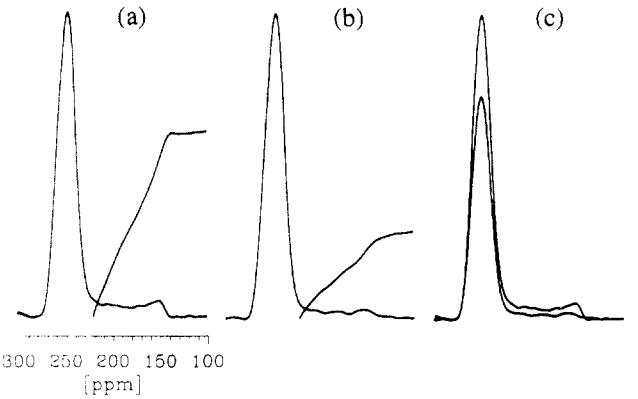

Figure 11. 1D exchange ^{13}C NMR spectra with selective saturation at T = 333 K. (a) On-resonance selection with the SELDOM technique (14 cycles with increasing precession delays for increased selectivity; sum of mixing times is 7 ms) at 260 ppm, near the low edge of the carboxyl powder pattern. The spectrum with its mixing time of 50 ms corresponds to a slightly broadened 1D cross section through the 2D exchange spectrum of Figures 4c or 12b at fixed $\omega_1 \approx 260$ ppm. The exchange intensity manifests itself in the low broad wing to the right of the selected line, with a small peak at ω_{22}. (b) MESSAGE spectrum directly analogous to the spectrum in a, taken with a total of 140 ms of mixing times for exchange and selective saturation (a 10-ms time after each of the 14 selection cycles of the SELDOM sequence). The integral traces plotted with the spectra show that the exchange intensity is suppressed by a factor of 2, proving a heterogeneous distribution of correlation times and a significant number of segments that are moving very little during a 50-ms mixing time. (c) Comparison of the spectra of a and b on an absolute intensity scale. The limited reduction of the overall intensity of the MESSAGE spectrum, in spite of the multiple saturation of the exchange intensity, again indicates a significant number of rigid segments.

Small-Amplitude Motions. In the ^2H 2D spectrum of Figure 9, the absence of a spectral component (Pake powder pattern) that is very narrow perpendicular to the diagonal indicates that there are only a few, if any, completely rigid units. This means that even the side groups that do not flip are undergoing restricted motions. These are taken into account in the simulation of Figure 9b by a restricted rotation around the local chain axis, with an average amplitude of (±)7°. Such small-amplitude excursions induced by molecular reorientations have also been observed in recent molecular dynamics simulations.[44] Note that the motions detected here most probably involve the main chain, since rotations around the C–C bond between the main chain and side group hardly reorient the methyl group and are therefore not detected in the ^2H 2D spectrum.

Significant line-shape changes on the diagonal are also observed in the ^{13}C NMR 2D spectra. Parts a and b of Figure 12 compare the stacked plots of ^{13}C 2D spectra at 233 and 333 K. While a perfect diagonal powder pattern is observed at the lower temperature, at 333 K the intensity at the edges of the spectrum, in particular at the ω_{33} end, is enhanced relative to other parts of the spectrum. As explained in the theoretical section above, this is characteristic of the frequency-dependent broadening caused by anisotropic small-angle reorientations. The ±7° rocking motion deduced from the ^2H 2D spectrum accounts only partially for the observed line shape. The experimentally observed effects in the ^{13}C 2D spectrum can be more closely approximated if additionally rotations around the local chain axis, with ca. 12° rms amplitude, are assumed for 25% of the side groups in the simulation (Figure 12d). These small-angle reorientations result naturally when, after two 180° flips, a given side group does not return exactly to its original orientation due to a change in its

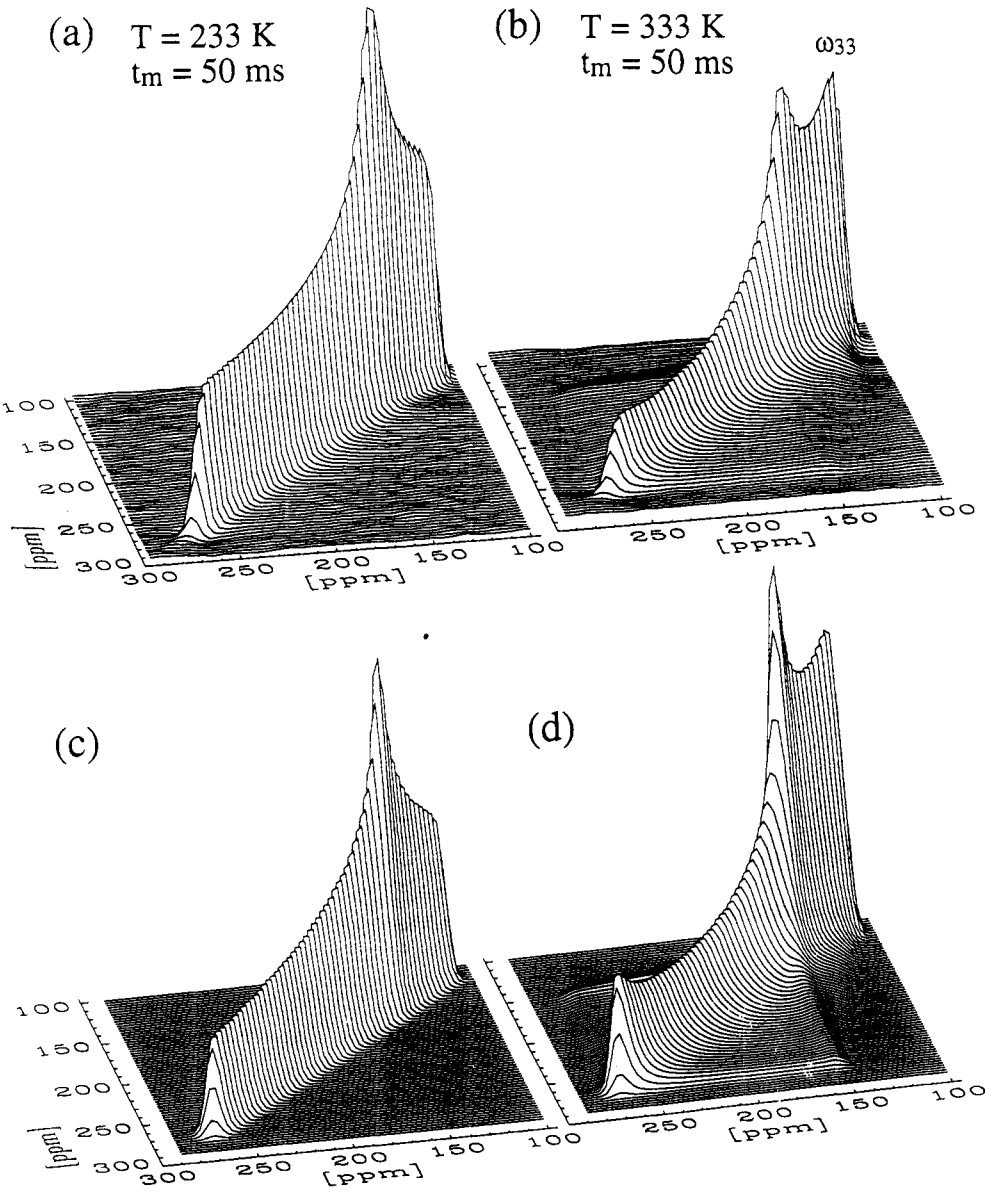

Figure 12. Stacked plots of ^{13}C exchange NMR spectra taken with t_m = 50 ms. (a) Diagonal powder pattern for T = 233 K. (b) At T = 333 K, significant changes of the intensity distribution on the diagonal are observed. The ω_{33} end of the spectrum is enhanced in part because the 180° inversion of the side group leaves this frequency invariant, but mainly due to small-angle motions around the normal of the OCO plane. They occur naturally when the side groups have flipped twice (see Figure 8d). (c) Simulated diagonal powder spectrum, corresponding to the experimental spectrum in a. (d) Stacked plot of the simulated spectrum of Figure 7c. Rotations around the ω_{33} direction with a root-mean-square amplitude of 12° are included in the model and produce changes in the line shape on the diagonal which are similar to those observed in the experimental spectrum in b.

environment. This is schematically displayed in Figure 8d. The change in the environment could be due to the rearrangement of the surrounding moieties caused by the slight misfit of the given asymmetric side group after the flip, or it might be caused by flips of other side groups within this environment, which also change the structure slightly. It should be noted that, in contrast to the small-angle rotations described here, the 20° rotations around the local chain axis that were discussed above always occur together with 180° side-group flips. In view of the complexity of the motional processes, the agreement between experimental and simulated 2D spectra is highly satisfying and we refrain from considering even more dynamical aspects in order to improve the fit further.

Summary of the Motional Processes. Figure 13 displays the overall reorientation-angle distributions of the carboxyl chemical-shift ω_z direction and the C_3 axis of the methoxy group, as used in the simulations of the ^{13}C and ^2H 2D spectra, respectively (Figures 7c or 12d and Figure 9b). Being derived from identical motional parameters, the differences in the distributions are only due to the different orientations of the two axes (see Figure 1a). In Figure 13, the components of the distributions are labelled "0", "1", and "2", according to the (minimum) number of flips that are required for the corresponding motions to occur. Component "0" represents the 50% of the side groups that only rock, with an average amplitude of 7°. Component 1 results from the 25% of the side groups that have undergone one 180° flip, or an odd number of flips, and concomitant reorientations around the normal of the OCO plane with a rms amplitude of 20°, which result from the asymmetry of the side group (see Figure 8c). Component 2 in the distributions, made up by another 25% of the groups, corresponds to two, or an even number, of flips with an effective rotation by typically 12° around the local chain axis. As indicated in Figure 8d, these reorientations are due to changes in the environment that are experienced by side groups that flip back to the vicinity of their original orientation.

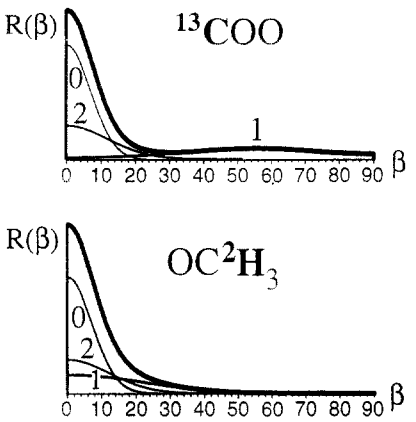

Figure 13. Reorientation-angle distributions $R(\beta)$ used in simulating the ^{13}C 2D NMR spectrum of Figure 7c/12d and the ^{2}H 2D NMR spectrum of Figure 9b. The underlying motional model is identical for both distributions. It consists of three motional processes. For simplicity, each of the three component distributions was assumed to be a Gaussian when considered over the full angular range of 360°. In the β-range of 90° that is accessible by NMR, the distributions may look asymmetric because contributions from the reorientation angles β, 180° − β, 180° + β, and 360° − β coincide. The component labeled 1 in the plot of the distribution function represents the 25% of the side groups that have flipped once (or $2N + 1$ times) and has a root-mean-square amplitude of 20°. Another 25% of the side groups have flipped back to the original orientation with an imprecision of 12° (two or $2N$ flips, labeled 2), and the remaining 50% are trapped but rock with an amplitude of ca. 7° (no flips, labeled 0). The maxima for the Gaussian distributions corresponding to component 1 are located at 8° and 54°, respectively, corresponding to twice the angle between the 180° flip axis and the z axis of the pertinent NMR interaction tensor.

Components 0 and 2 of the distributions reflect motions around the local chain axis, which are experienced in similar ways by the two NMR probes, ^{13}C and ^{2}H, in the side group. The only difference between the distributions in Figure 13a,b is observed for the 180°-flip component 1. The maximum of this component appears at an angle which is twice the angle between the flip axis and the z axis of the interaction probed. For the carboxyl chemical shift, this maximum is at 2 × 27° = 54°; for the deuterated methoxy group it occurs at 2 × 4° = 8°.

Relation to Mechanical Relaxation. Due to the asymmetry of the side group, its motion occurs between energetically inequivalent sites; therefore, it is mechanically active. Our spectra show that the side-group dynamics are accompanied by main-chain motion, and we can quantify the corresponding motional amplitudes to be as large as (±)20°, in particular through the combination of the ^{13}C and ^{2}H data. The ω_{33} features of the ^{13}C 2D NMR spectra show that rearrangements of the main chain, which result in an effective rotation around the local chain axis, are at least as important in the energy minimization as are deviations from the 180° angle of the side-group motion. This indicates the dominance of steric interactions between different segments, compared to intramolecular bond-rotation potentials. The latter are sometimes overemphasized in the descriptions of localized motions and corresponding simple computer simulations. Advanced molecular dynamics approaches[44] to relaxations in polymers do actually take matrix effects into account.

The large-angle main-chain motions which are caused by the reorientation of the asymmetric side group in PMMA are not observed for other β-type processes in the glassy state, such as phenylene-ring flips in polycarbonates[20] and in liquid-crystalline side-group polymers.[21] There, no evidence is found for a coupling of the flip to significant (>10°) reorientations of the phenylene-ring axis. This is not too surprising because the phenylene ring, being symmetric, flips between two sterically equivalent positions and therefore does not require a long-term rearrangement of its axis or the environment. Only during the flip would transient structural changes be necessary.

Having proved that the molecular origin of the β relaxation in PMMA is a large-amplitude side-group flip and a concomitant main-chain torsion, we can understand qualitatively why the β-relaxation strength is quite strongly reduced by applied pressure[45,46] and by changes in the local environment of the side groups, such as removal of the main-chain methyl group,[6] copolymerization,[47] or isotactic chain configurations.[1] While the packing around the side groups is "loose" enough in atactic or syndiotactic PMMA at normal pressure to permit side-group flips, unfavorable changes can easily quench that motion and its influence on the main-chain dynamics. It should also be noted that X-ray studies of PMMA have shown anomalous behavior indicating a notable degree of packing regularity in this polymer.[48]

(5) Summary and Outlook

We have elucidated the molecular rotations underlying the β relaxation in PMMA by means of 2D and selective-excitation 3D exchange NMR techniques, using ^{13}C chemical-shift and ^{2}H quadrupolar anisotropies as complementary probes of dynamical information. The 2D and selective 3D spectra show that 180° side-group flips occur, with no more than 20° rms deviation in the flip angle. The flips are accompanied by rotational readjustments with an amplitude of ca. ±20° around the local chain axis. In a consecutive jump, the side group returns to its original orientation with a precision of ca. 12°. Multiple selective saturation and exchange experiments prove that a wide distribution of correlation times is present in the sample. Consistently, integration of the exchange intensity shows that only about 50% of the segments partake in the large-angle dynamics on the time scale observed in the experiments, while the other 50% only undergo rocking motions around the local chain axis, with an amplitude of approximately 7°. The correlation times determined from the NMR spectra confirm the identification of the reorientations observed by exchange NMR with the β-relaxation dynamics.

The anisotropic molecular dynamics of the side group above T_g and the merging of the β and α relaxations have been studied recently in our laboratory for PEMA,[42,43] by means of the techniques described in this paper. Studies of the main-chain motions as probed directly by deuterium labels on the main chain are currently underway. Further on, it may be interesting to investigate details of the distribution of correlation times and the fraction of trapped side groups by systematically studying the mixing-time dependence of the exchange intensity, and by application of the MESSAGE experiment. These aspects are also relevant in the characterization of the β relaxations in other methacrylates, acrylates, and methacrylate copolymers.

Acknowledgment. Financial support by the Deutsche Forschungsgemeinschaft (SFB 262) is gratefully acknowledged. H.W.B. thanks the National Science Foundation for a NSF–NATO postdoctoral fellowship. A.S.K. thanks the Max Planck Society for a stipend. A donation of the Dr. Otto Röhm Gedächtnisstiftung is highly appreciated.

References and Notes

(1) McCrum, N. G.; Read, B. E.; Williams, G. *Anelastic and Dielectric Effects in Polymeric Solids*; Wiley: New York, 1967.

(2) Roetling, J. A. *Polymer* **1965**, *6*, 311.
(3) Boyd, R. H.; Robertson, M. E.; Jansson, J. F. *J. Polym. Sci., Polym. Phys. Ed.* **1982**, *20*, 73.
(4) Diaz-Calleja, R.; Ribes-Greus, A.; Gomez-Ribelles, J. *Polymer* **1989**, *30*, 1433.
(5) Reference 1, p 246.
(6) Heijboer, J.; Baas, J. M. A.; van de Graaf, B.; Hoefnagel, M. A. *Polymer* **1987**, *28*, 509.
(7) Reference 1, p 178.
(8) Desando, M. A.; Kashem, M. A.; Siddiqui, M. A.; Walker, S. *J. Chem. Soc., Faraday Trans. 2* **1984**, *89*, 747.
(9) Tsay, F.-D.; Gupta, A. *J. Polym. Sci., Part B: Polym. Phys.* **1987**, *25*, 855.
(10) Johari, G. P.; Goldstein, M. *J. Chem. Phys.* **1971**, *55*, 4245.
(11) Muzeau, E.; Perez, J.; Johari, G. P. *Macromolecules* **1991**, *24*, 4713.
(12) Jeener, J.; Meier, B. H.; Bachmann, P.; Ernst, R. R. *J. Chem. Phys.* **1979**, *71*, 4546.
(13) Ernst, R. R.; Bodenhausen, G.; Wokaun, A. *Principles of Nuclear Magnetic Resonance in One and Two Dimensions*; Clarendon Press: Oxford, U.K., 1987.
(14) Schmidt, C.; Wefing, S.; Blümich, B.; Spiess, H. W. *Chem. Phys. Lett.* **1986**, *130*, 84. Schmidt, C.; Blümich, B.; Spiess, H. W. *J. Magn. Reson.* **1988**, *79*, 269.
(15) Wefing, S.; Spiess, H. W. *J. Chem. Phys.* **1988**, *89*, 1219.
(16) Hagemeyer, A.; Schmidt-Rohr, K.; Spiess, H. W. *Adv. Magn. Reson.* **1989**, *13*, 85.
(17) Schaefer, D.; Spiess, H. W.; Suter, U. W.; Fleming, W. W. *Macromolecules* **1990**, *23*, 3431.
(18) Kaufmann, S.; Wefing, S.; Schaefer, D.; Spiess, H. W. *J. Chem. Phys.* **1990**, *93*, 197.
(19) Schmidt-Rohr, K.; Spiess, H. W. *Multidimensional Solid-State NMR and Polymers*; Academic Press: London, New York, 1994.
(20) Hansen, M. T.; Blümich, B.; Boeffel, C.; Spiess, H. W.; Morbitzer, L.; Zembrod, A. *Macromolecules* **1992**, *25*, 5542. Hansen, M. T.; Boeffel, C.; Spiess, H. W. *Colloid Polym. Sci.* **1993**, *271*, 446.
(21) Leisen, J.; Boeffel, C.; Dong, R. Y.; Spiess, H. W. *Liq. Cryst.* **1993**, *14*, 215.
(22) Spiess, H. W. *Colloid Polym. Sci.* **1983**, *261*, 193; *Adv. Polym. Sci.* **1985**, *66*, 23.
(23) Inglefield, P. T.; Amici, R. M.; O'Gara, J. F.; Hung, C.-C.; Jones, A. A. *Macromolecules* **1983**, *16*, 1552. O'Gara, J. F.; Jones, A. A.; Hung, C.-C.; Inglefield, P. T. *Macromolecules* **1985**, *18*, 1117.
(24) Schaefer, J.; Stejskal, E. O.; McKay, R. A.; Dixon, W. T. *Macromolecules* **1984**, *17*, 1749.
(25) Schmidt-Rohr, K.; Spiess, H. W. *Proc. XXV Congr. Ampere* **1990**, 512.
(26) Spiess, H. W.; Schmidt-Rohr, K. *Polym. Prepr. (Am. Chem. Soc., Div. Polym. Chem.)* **1992**, *33* (1), 68.
(27) Pines, A.; Gibby, M. G.; Waugh, J. S. *J. Chem. Phys.* **1973**, *59*, 569.
(28) Cox, R. F. B.; Stormant, R. T. *Organic Syntheses*; Wiley: New York, 1945; Collect. Vol. II, p 6.
(29) Naarmann, H., private communication.
(30) Haeberlen, U. *Advances in Magnetic Resonance. Supplement 1*; Academic Press: New York, 1976.
(31) Veeman, W. S. *Prog. NMR Spectrosc.* **1984**, *16*, 193.
(32) Kulik, A.; Spiess, H. W. *Makromol. Chem.* **1994**, *195*, 1755.
(33) Tekely, P.; Brondeau, J.; Elbayed, K.; Retournard, A.; Canet, D. *J. Magn. Reson.* **1988**, *80*, 509.
(34) Schmidt-Rohr, K.; Spiess, H. W. *Phys. Rev. Lett.* **1991**, *66*, 3020.
(35) Leisen, J.; Schmidt-Rohr, K.; Spiess, H. W. *Physica A* **1993**, *201*, 79; *J. Non-Cryst. Solids*, in press.
(36) Caravatti, P.; Levitt, M. H.; Ernst, R. R. *J. Magn. Reson.* **1986**, *68*, 323.
(37) Gomez Ribelles, J. L.; Diaz Calleja, R. *J. Polym. Sci., Polym. Phys. Ed.* **1985**, *23*, 1297.
(38) Lovell, R.; Windle, A. *Polymer* **1981**, *22*, 175.
(39) Coiro, V. M.; De Santis, P.; Liquori, A. M.; Mazzarella, L. *J. Polym. Sci., Part C* **1969**, *16*, 4591.
(40) Vacatello, M.; Flory, P. J. *Macromolecules* **1986**, *19*, 415.
(41) Hagemeyer, A.; Brombacher, L.; Schmidt-Rohr, K.; Spiess, H. W. *Chem. Phys. Lett.* **1990**, *167*, 583.
(42) Kulik, A. S.; Radloff, D.; Spiess, H. W. *Macromolecules* **1994**, *27*, 3111.
(43) Kulik, A. S.; Beckham, H. W.; Schmidt-Rohr, K.; Radloff, D.; Pawelzik, U.; Boeffel, C.; Spiess, H. W. *Macromolecules*, following paper in this issue.
(44) Hutnik, M.; Argon, A. S.; Suter, U. W. *Macromolecules* **1991**, *24*, 5970.
(45) Koppelmann, J. *Prog. Colloid Polym. Sci.* **1979**, *66*, 235.
(46) Fytas, G.; Patkowski, A.; Meier, G.; Dorfmüller, Th. *J. Chem. Phys.* **1984**, *80*, 2214.
(47) Mashimo, S.; Yagira, S.; Iwasa, Y. *J. Polym. Sci., Polym. Phys. Ed.* **1978**, *16*, 1761.
(48) Miller, R. L.; Boyer, R. F.; Heijboer, J. *J. Polym. Sci., Polym. Phys. Ed.* **1984**, *22*, 2021.